available at www.sciencedirect.com

ScienceDirect

journal homepage: www.elsevier.com/locate/chnjc

Article

Density functional theory study of the adsorption and reaction of C_2H_4 on $Fe_3C(100)$

Bingyin Wang [a,b], Xiaohu Yu [a], Chunfang Huo [a,c,*], Jianguo Wang [a], Yongwang Li [a,c]

[a] *State Key Laboratory of Coal Conversion, Institute of Coal Chemistry, Chinese Academy of Sciences, Taiyuan 030001, Shanxi, China*
[b] *University of Chinese Academy of Sciences, Beijing 100049, China*
[c] *National Energy R&D Center for Coal to Liquid Fuels, Synfuels China Co. Ltd, Beijing 101407, China*

ARTICLE INFO

Article history:
Received 29 July 2013
Accepted 2 September 2013
Published 20 January 2014

Keywords:
Ethylene
Cementite
Adsorption
Dehydrogenation
Cleavage
Fischer-Tropsch synthesis
Density functional theory

ABSTRACT

Spin-polarized density functional theory (DFT) and a periodic slab model were employed to investigate the adsorption of C_2H_4 on $Fe_3C(100)$, which is an active phase of an Fe-based catalyst for Fischer-Tropsch synthesis. The competition between dehydrogenation and cleavage of C_2H_4 was analyzed. The μ-bridging adsorption mode is more stable than the π or di-σ adsorption modes. Partial rehybridization of the C atoms of C_2H_4 ($sp^2 \rightarrow sp^3$) caused by the interaction of C_2H_4 with the $Fe_3C(100)$ surface resulted in the C atoms in C_2H_4 having a quasi-tetrahedron geometry. On $Fe_3C(100)$ dehydrogenation of C_2H_4 occurs, while C–C bond cleavage is not competitive. The calculations indicated that vinylidene (CCH_2) and vinyl ($CHCH_2$) species are the most abundant C_2 species, which may be the major monomeric forms of C_2H_4 in the chain growth in Fischer-Tropsch synthesis.

1. Introduction

Fischer-Tropsch synthesis [1] is used to convert syngas (CO + H_2) into hydrocarbons. It is a crucial catalytic process for transforming coal, natural gas, and biomass into high quality liquid fuels and chemical resources. Iron-based catalysts possess the following advantages: wide operating temperature range, high space time yield and alkene yield, high water-gas shift activity, and low price [2]. They are studied and applied extensively [3].

Many transmission electron microscopy, X-ray diffraction, and Mössbauer spectroscopy experiments have shown that iron carbides, including Fe_5C_2 and Fe_3C [4–9], are the main active phases of iron-based catalysts in FTS. Although significant progress has been made in experimental and theoretical investigations in recent years, there remain some critical scientific issues not yet resolved. For example, how does the hydrocarbon chain grow [10]? How does alkene readsorption affect the product distribution? Until now, three chain propagation mechanisms have been proposed for FTS: carbide mechanism [11], hydroxy-carbene mechanism [12,13], and CO insertion mechanism [14]. Many experimental and theoretical results have verified the existence of C_xH_y species on many metal surfaces [15,16], which give strong support for the carbide mechanism.

In the traditional carbide mechanism, CH_2 is considered the monomer for chain growth. However, different opinions have been proposed in recent years. Ciobica et al. [17] found that CH

* Corresponding author. Tel: +86-10-69667589; Fax: +86-10-69667800; E-mail: hcf905@sxicc.ac.cn
This work was supported by the National Basic Research Program of China (973 Program, 2011CB201401) and the National Natural Science Foundation of China (21273261).
DOI: 10.1016/S1872-2067(12)60703-7 | http://www.sciencedirect.com/science/journal/18722067 | Chin. J. Catal., Vol. 35, No. 1, January 2014

was the most stable C_1 species on Ru(0001), and they suggested that CH was the chain propagation monomer, which agreed with the experimental results of Wu et al. [18,19]. Liu et al. [20,21] carried out density functional theory (DFT) calculations to investigate C–C coupling reactions on both flat and stepped Ru(0001) and stepped Rh(111), and also used CH as the carbon chain growth monomer on stepped Ru(0001) and Rh(111). Deng et al. [22] found that the most stable CH_x species on $Fe_3C(100)$ was CH, and that it was mostly derived from the hydrogenation of surface C atoms, with a small quantity supplied by hydrogen-assisted CO disassociation.

Krishna et al. [23] studied the effect of the presence of C_2H_4 on the product distribution by using $^{13}CO/H_2$ and $^{12}C_2H_4$. They found that the proportion of C_{3+} hydrocarbons in the product was increased by C_2H_4 readsorption. Cao et al. [24] carried out DFT calculations and proposed that the CCH species from the dehydrogenation of CCH_2 and CHCH coupled with C atoms to form CCCH on $Fe_5C_2(001)$. The experimental results of Turner et al. [25,26] and Jordan et al. [27] indicated that vinyl species ($CHCH_2$) participated in the formation of hydrocarbons as the chain growth monomer. Using the investigation of high molecular weight hydrocarbon formation on a Ru catalyst, Mims et al. [28] concluded that vinylidene (CCH_2) was the stable monomer C_2 species.

In this paper, we employed spin-polarized DFT and a periodic slab model to investigate the thermodynamics and kinetics of the adsorption, dehydrogenation, and cleavage of C_2H_4 on $Fe_3C(100)$. The aims were to elucidate the nature of C_2H_4 readsorption, what are the possible monomeric forms that take part in the chain propagation in FTS, and to give guidelines for further kinetic studies.

2. Method and surface model

All calculations were performed using the plane wave periodic density functional method implemented in the Vienna *ab initio* simulation package (VASP) [29–31]. Exchange and correlation energies were calculated using the Perdew, Burke, and Ernzerhof (PBE) functional [32] in the generalized gradient approximation (GGA). The electron-ion interaction was described by the projector augmented wave (PAW) [33], and the Kohn-Sham one-electron states up to 400 eV were expanded using a plane wave basis set. Due to its large effect on a magnetic system, spin polarization was included for super-paramagnetic cementite (Fe_3C) to correct the calculations.

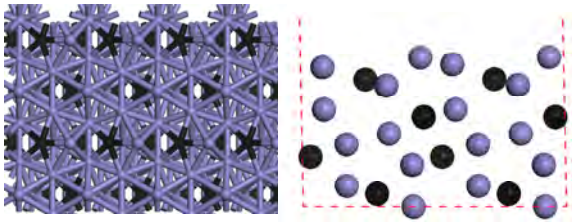

Fig. 1. Top and side views of the $Fe_3C(100)$ surface. Fe atoms in blue; C atoms in black.

A 1×3×1 K-point sampling within the Brillouin zone was used in the p(1×2) and p(2×2) unit cell of the periodic slab model to investigate the adsorption, dehydrogenation, and cleavage of C_2H_4 on $Fe_3C(100)$. The slab (without adsorbates) vacuum was set to span 1.5 nm to exclude the interactions between the periodic slabs. As illustrated in Fig. 1, a slab consisting of eight Fe layers and four C layers (8Fe + 4C) was employed.

In all calculations, the bottom six Fe layers and three C layers (6Fe + 3C) were fixed at their bulk position, while the top two Fe layers and one C layer were allowed to relax. For evaluating energy barriers, all transition states were located using the climbing image-nudged elastic band (CI-NEB) method [34]. All stable configurations and transition states were verified by vibrational frequency analysis. The adsorption energy was defined as $E_{ads} = E(\text{adsorbates/slab}) - [E(\text{adsorbates}) + E(\text{slab})]$, where E(adsorbates/slab) is the total energy of the slab with adsorbates, E(adsorbates) is the total energy of the free adsorbates, and E(slab) is the total energy of the bare slab. The reaction energy and barrier were calculated by $\Delta_r E = E(\text{FS}) - E(\text{IS})$ and $E_a = E(\text{TS}) - E(\text{IS})$, where E(IS), E(TS), and E(FS) are the energies of the corresponding initial state (IS), transition state (TS), and final state (FS), respectively.

3. Results and discussion

3.1. C_2H_4 adsorption

All possible C_2H_4 adsorption sites on the $Fe_3C(100)$ surface were considered systematically, and three adsorption modes, π, di-σ, and μ-bridging, were found. The calculated stable adsorption structures, key bond parameters, and adsorption energies are given in Fig. 2.

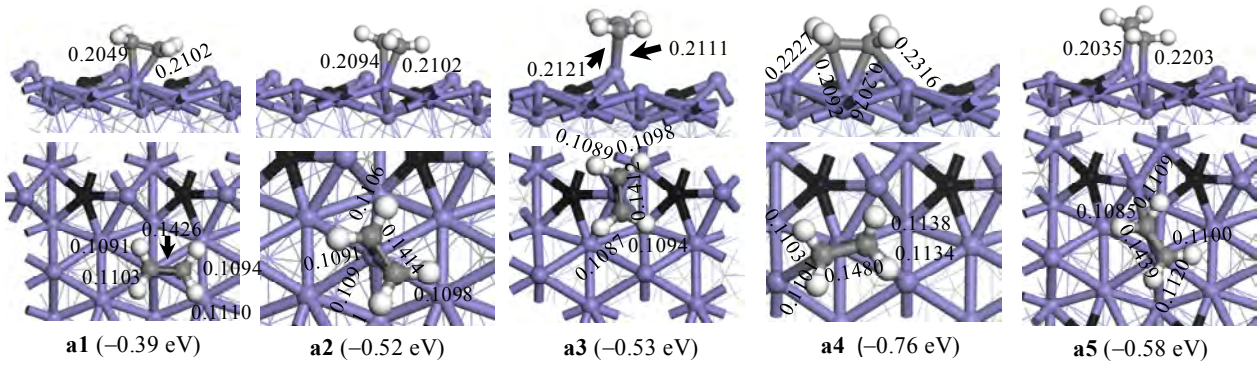

Fig. 2. C_2H_4 adsorption on $Fe_3C(100)$. Fe atoms in blue; C atoms in black; C atoms of C_2H_4 in gray; H atoms of C_2H_4 in white.

In configurations **a1**, **a2**, and **a3**, C_2H_4 adsorbs on the exposed first Fe layers by π coordination. The C and H atoms of C_2H_4 are in approximately the same plane, while both the two C atoms bond with the same Fe atom in the substrate to form a σ-π compound with a three-membered C–Fe–C ring structure [35]. The adsorption energies of three configurations are –0.39, –0.52, and –0.53 eV. In comparison with the C–C bond length (0.1330 nm) of C_2H_4 in gas phase, the C–C bond distance is elongated to 0.1426, 0.1414, and 0.1412 nm, indicating that the C–C bond strength is weakened. Because $Fe_3C(100)$ is a rough surface, adsorbed C_2H_4 in configuration **a2** is tilted slightly, leading one of its C atoms to interact with another surface Fe atom to give the quasi di-σ adsorption configuration **a5**. In this configuration, the C–C bond length (0.1439 nm) is weakened further. The adsorption energy of –0.58 eV is close to those of **a2** and **a3**, with small differences of –0.06 and –0.05 eV. In configuration **a4**, both C atoms bridge a first layer and a second layer Fe atom, forming a μ-bridging adsorption mode. It is the most stable structure for C_2H_4 on $Fe_3C(100)$ with the adsorption energy of –0.76 eV, in which the C–C bond is highly activated with the distance of 0.1480 nm, which is between that of C_2H_4 (0.1330 nm) and C_2H_6 (0.1540 nm). The four H atoms from the C–C plane have the H–C–C angle of 114°, which is between that of C_2H_4 (121°) and C_2H_6 (111°). This showed that in the μ-bridging mode, the C atoms of C_2H_4 have been partially rehybridized from sp^2 to sp^3 to give the C atoms a quasi-tetrahedron geometry.

In summary, ethylene adsorbs weakly on $Fe_3C(100)$ surface, and the μ-bridging adsorption mode with a highly activated C–C double bond is more stable than the π and di-σ adsorption modes, which is similar to the adsorption behavior of C_2H_4 on metal surfaces [36,37]. At low coverages, ethylene C_2H_4 mainly adsorbs in the μ-bridging mode. At high coverages, all five C_2H_4 adsorption configurations can coexist. The highest occupied molecular orbital (HOMO) of ethylene is the bonding π orbital. The lowest unoccupied molecular orbital (LUMO) is the antibonding π* orbital. When adsorbed on Fe atoms, ethylene transfers part of its electrons of the bonding π orbital to the 3*d* empty orbital of Fe atoms. At the same time, the antibonding π* orbital energy is decreased to receive the backbonding electrons of the 3*d* orbital of the Fe atoms. Both interactions cooperatively enhance the interactions between ethylene and the surface, and thus weaken the ethylene C=C double bond, making the bond length elongated and the bond order lower.

3.2. C_2H_4 dehydrogenation and cleavage on $Fe_3C(100)$

Dehydrogenation and C–C cleavage are competitive reactions for C_2H_4 on $Fe_3C(100)$. It was reported that a number of surface reactions obey the Brönsted-Evans-Polanyi (BEP) relationship [38,39], that is, the weaker adsorption configuration has the higher reactivity. On the other hand, the stronger adsorption configuration has the higher surface concentration. We chose the **a1** configuration (Fig. 2**a1**) in the π adsorption mode and **a4** configuration in the μ-bridging adsorption mode to investigate the stepwise dehydrogenation and cleavage of ethylene on the $Fe_3C(100)$ surface. Because the **a2** and **a3** configurations have the same adsorption modes as the **a1** configuration, and the **a5** configuration can be obtained from the **a2** configuration, the **a2**, **a3**, and **a5** configurations would have a similar reaction behavior as the **a1** configuration. The reaction energies and energy barriers of all possible elementary reactions are given in Table 1. The key structures of the intermediates and transition states in the optimized dehydrogenation and cleavage pathways are displayed in Fig. 3.

3.2.1. Dehydrogenation and cleavage of configuration ***a1*** *(C_2H_4)*

Because four H atoms of C_2H_4 are in different surface environments, each dehydrogenation step is selective. From the energy data in Table 1, with configuration **a1** as the starting point, the dehydrogenating energies for the loss of one H atom among the $H_{a\text{-}d}$ ($C_2H_4 \rightarrow C_2H_3 + H$) are quite different. Dehydrogenating H_a is kinetically most favored. It is slightly exothermic by 0.08 eV and has a barrier of 0.34 eV. In the transition state **TS(a1/b1)**, the bond length of C_1–H_a is elongated from 0.1095 nm in the initial adsorption state to 0.1541 nm. H_a occupies an on-top site Fe atom with the Fe–H_a length of 0.1611 nm. In the final state **b1**, the H atom adsorbs on the 3-fold site composed of first layer and second layer Fe atoms with the Fe–H_a bond lengths of 0.1744, 0.1784, and 0.1880 nm. The **a1** cleavage process ($C_2H_4 \rightarrow 2CH_2$) was predicted to be exothermic by 0.18 eV and has an energy barrier of 1.55 eV. In the transition state **TS(a1/c1)**, the C–C bond length is elongated to 0.2393 nm (0.1414 nm in the initial adsorption state). In the final state **c1**, the C–C bond is completely broken, and CH_2 adsorbs on the deep hollow site composed of one first layer Fe atom and two second layer Fe atoms. For C_2H_4 (**a1**) on the $Fe_3C(100)$ surface, dehydrogenation occurs first to form an adsorbed vinyl $CHCH_2$ species.

As compared with the first step of C_2H_4 dehydrogenation and cleavage, the corresponding energy barrier of **b1** dehydrogenation ($C_2H_3 \rightarrow C_2H_2 + H$) and cleavage ($C_2H_3 \rightarrow CH_2 + CH$) were decreased obviously (0.06 vs 0.47 eV, 0.55 vs 1.50 eV, and 0.67 vs 1.55 eV). Dehydrogenating the H_b atom is more favored kinetically. The CH group in $CHCH_2$(**b1**) tilts towards to the

Table 1
Activation barriers and reaction energies (eV) for C_2H_4 dehydrogenation and cleavage on $Fe_3C(100)$.

Reaction	Elementary step	E_a(**a1**) /eV	ΔE_r(**a1**) /eV	E_a(**a4**) /eV	ΔE_r(**a4**) /eV
$C_2H_4 \rightarrow C_2H_3 + H$	Dehy-H_a	0.34	–0.08	0.58	0.06
	Dehy-H_b	0.47	–0.08	0.64	0.08
	Dehy-H_c	1.50	–0.26	1.01	–0.28
	Dehy-H_d	1.06	–0.26	0.93	0.74
$C_2H_4 \rightarrow 2CH_2$	Cleavage	1.55	–0.18	1.40	1.13
$C_2H_3 \rightarrow C_2H_2 + H$	Dehy-H_a				
	Dehy-H_b	0.06	–0.27	0.58	0.08
	Dehy-H_c	0.55	0.22	0.62	–0.01
	Dehy-H_d			0.90	0.01
$C_2H_3 \rightarrow CH + CH_2$	Cleavage	0.67	–0.35	0.74	0.38
$CCH_2 \rightarrow CH + H$	Dehy-H_a				
	Dehy-H_b				
	Dehy-H_c	1.10	0.80	0.74	0.28
	Dehy-H_d	1.12	0.80	0.92	0.26
$CCH_2 \rightarrow C + CH_2$	Cleavage	1.69	0.81	0.88	0.81

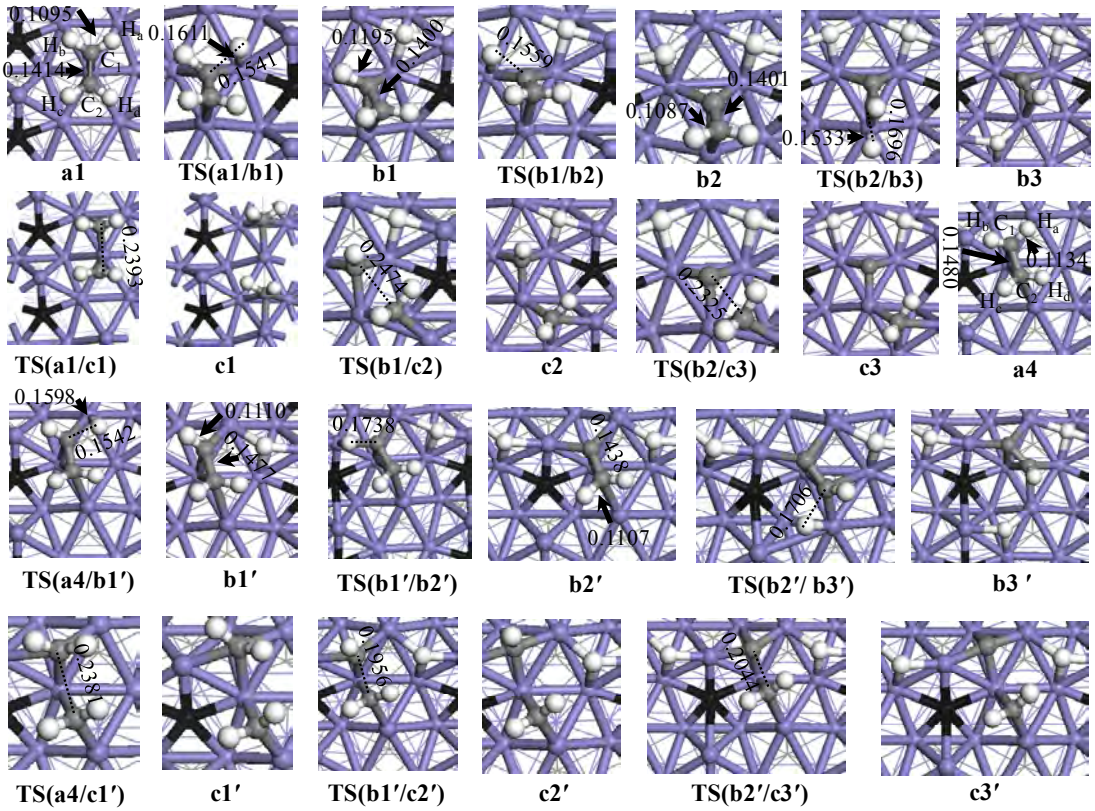

Fig. 3. Structures of key intermediates involved in the most favored C_2H_4 dehydrogenation and cleavage pathways on $Fe_3C(100)$.

surface, which promotes C–H activation. In the transition state **TS(b1/b2)**, the bond length of C_1–H_b is stretched from 0.1195 nm in adsorption state **b1** to 0.1559 nm, and the H_b atom adsorbs on the top of a Fe atom with the Fe–H_b distance of 0.1602 nm. In the final state **b2**, the H_b atom resides on the 3-fold site composed of the first and second layer Fe atoms with the Fe–H_b distances of 0.1691, 0.1710, and 0.1897 nm. This reaction is exothermic by 0.27 eV and only needs a barrier of 0.06 eV to form the vinylidene species in the $\eta^3\eta^1$(C,C) adsorption mode. In the transition state **TS(b1/c2)** for the **b1** cleavage reaction ($C_2H_3 \rightarrow CH_2 + CH$), the C–C bond length is elongated to 0.2474 nm (0.1400 nm in **b1**), and the barrier is 0.67 eV. In the final state **c2**, the C–C bond is totally broken to form CH and CH_2 species on 3-fold sites. This process is exothermic by 0.35 eV.

Due to the approximate symmetry for configuration **b2**(CCH_2) relative to the vertical surface and the C–C bond, dehydrogenating the H_c and H_d atoms have close reaction energies (0.80 and 0.80 eV) and barriers (1.10 and 1.12 eV). In the transition state **TS(b2/b3)**, the C_2–H_c bond is elongated from 0.1087 nm to 0.1696 nm, and H_c is located on the top site of a Fe atom with the Fe–H_c bond of 0.1533 nm. In final state **b3**, the acetylidene specie (CCH) is adsorbed in the $\eta^3\eta^1$(C,C) mode, and the H_c atom occupies the 3-fold site with the Fe–H_c bond of 0.1700, 0.1823, and 0.1971 nm. The cleavage reaction ($CCH_2 \rightarrow C + CH_2$) for **b2** was calculated to be endothermic by 0.81 eV with a barrier of 1.69 eV. In the transition state **TS(b2/c3)**, the C–C bond length is elongated to 0.2325 nm (0.1401 nm in **b2**). In the final cleavage product **c3**, C and CH_2 adsorbs at η^3 sites composed of one first layer Fe atom and two second Fe atoms or two first layer Fe atoms and one second layer Fe atom.

From the energy profile of the dehydrogenation and cleavage of configuration **a1** in Fig. 4, we can see that for C_2H_4 on $Fe_3C(100)$, dehydrogenation easily occurs, while C–C bond cleavage is not competitive. Vinylidene (CCH_2) is the most stable C_2 species on the surface, with the first and second dehydrogenation steps having low energy barriers of 0.34 and 0.06 eV, respectively. However, the following dehydrogenation of vinylidene (CCH_2) needs to overcome a high energy barrier of 1.10 eV and it is endothermic by 0.80 eV. This indicated that vinylidene (CCH_2) dehydrogenation was difficult under FTS conditions. In contrast, acetylidene (CCH) can be hydrogenated

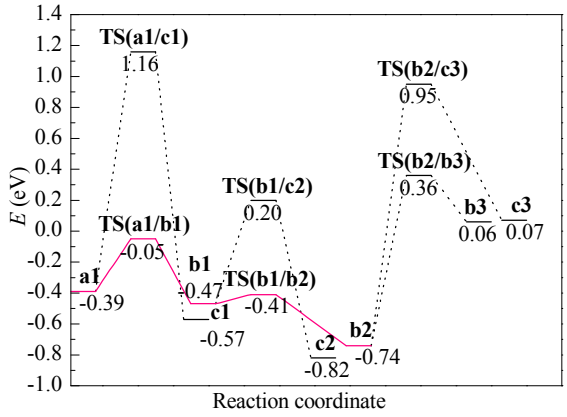

Fig. 4. Energy profiles for the most favored dehydrogenation and cleavage pathways of C_2H_4 (**a1**) on $Fe_3C(100)$. The most favored pathway is indicated by the solid line.

to form the vinylidene (CCH_2) species, which is exothermic by 0.80 eV with a relatively low barrier of 0.30 eV.

3.2.2. Dehydrogenation and cleavage of configuration ***a4*** (C_2H_4)

Taking configuration **a4** as the starting point, dehydrogenating the H_a atom ($C_2H_4 \rightarrow C_2H_3 + H_a$) is kinetically the most favored first step with a total energy barrier of 0.58 eV, as illustrated in Table 1. At the beginning, H_a atom moves gradually far away from the C_1 atom, tilting towards to the surface. In the transition state **TS(a4/b1′)**, the bond length of C_1–H_a is elongated to 0.1542 nm (0.1134 nm in the initial state). Meanwhile, the H_a atom resides on the top site with the Fe–H_a length of 0.1598 nm. In the final state **b1′**, H_a occupies the 3-fold site consisting of first layer and second layer Fe atoms with the Fe–H_a length of 0.1741, 0.1841, and 0.1851 nm. This step is endothermic by 0.06 eV. The **a4** cleavage ($C_2H_4 \rightarrow 2CH_2$) was predicted to be endothermic by 1.13 eV and had a barrier of 1.40 eV. In the transition state **TS(a4/c1′)**, the C–C distance is elongated from 0.1480 nm in the initial adsorption state to 0.2381 nm. In the final state **c1′**, the C–C bond is completely broken to form two CH_2 groups in the 3-fold site and the bridge site. This indicated that on $Fe_3C(100)$, C_2H_4 (**a4**) preferred dehydrogenation to form the vinyl $CHCH_2$ (**b1′**) species.

In the following step, dehydrogenating the H_b atom to form vinylidene CCH_2 (**b2′**) presents a lower energy barrier (0.58 vs 0.62 eV) than dehydrogenating the H_c atom to form acetylene CHCH (**b2″**). In the transition state **TS(b1′/b2′)**, the C_1–H_b bond is elongated to 0.1738 nm (0.1110 nm in **b1′**). H_b atom adsorbs on the top site of an adjacent surface Fe atom with the Fe–H_b bond length of 0.1546 nm. In the final state **b2′**, H_b atom occupies the shallow hollow site with the Fe–H_b bond lengths of 0.1704, 0.1877, and 0.1987 nm. The formation of vinylidene (CCH_2) is endothermic by 0.08 eV. In the transition state **TS(b1′/c2′)** corresponding to the cleavage of configuration **b1′** ($C_2H_3 \rightarrow CH_2 + CH$), the C–C bond is elongated to 0.1956 nm (0.1477 nm in **b1′**). In the final state **c2′**, the C–C bond is entirely broken. CH_2 resides on the bridge site composed of one first and one second layer Fe atoms, while CH occupies the 3-fold site formed by two first layer Fe atoms and one second layer Fe atom. This step is endothermic by 0.38 eV and has an energy barrier of 0.74 eV.

The dehydrogenation product **b2′** of configuration **a4** adsorbs on the $Fe_3C(100)$ surface in the $\eta^2\eta^3$(C,C) mode, with the H_c and H_d atoms situated in different surface environments. The energy barrier of dehydrogenating H_c ($CCH_2 \rightarrow CCH + H_c$) differs from that of H_d atom (0.74 vs 0.92 eV). In the transition state **TS(b2′/b3′)**, the C_2–H_c bond is stretched from 0.1107 to 0.1706 nm, and the H_c atom moves away to the top site of a Fe atom with the Fe–H_c distance of 0.1648 nm. In the final state **b3′**, acetylidene (CCH) is located on the $\eta^3\eta^3$(C,C) site, and the H_c atom adsorbs on a 3-fold site formed by two first layer Fe atoms and one second layer Fe atom with the Fe–H_c bond length of 0.1721, 0.1873, and 0.1926 nm. This step is endothermic by 0.28 eV. **b2′** cleavage ($CCH_2 \rightarrow C + CH_2$) has an energy barrier of 0.88 eV and is endothermic by 0.81 eV. In the transition state **TS(b2′/c3′)**, the C–C bond length is elongated to 0.2044 nm (0.1438 nm in **b2′**). In the final cleavage product **c3′**, C resides on the 4-fold site composed of two first and two second layer Fe atoms, and CH_2 occupies the bridge site formed by one first and one second layer Fe atoms.

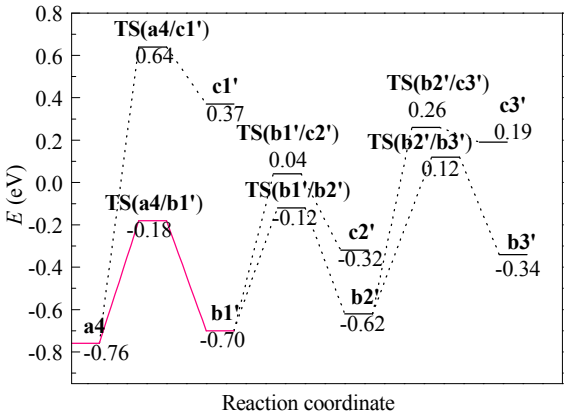

Fig. 5. Energy profiles for the most favored dehydrogenation and cleavage paths of C_2H_4(**a4**) on $Fe_3C(100)$. The most favored pathway is indicated by the solid line.

From the energy profiles in Fig. 5 for the dehydrogenation and cleavage of configuration **a4** in the μ-bridging mode, we can see that the energy barrier for C–C cleavage is much higher than that for dehydrogenation, and thus dehydrogenation would occur. The three dehydrogenation steps have close energy barriers of 0.58, 0.58, and 0.74 eV, and are endothermic by 0.06, 0.08, and 0.28 eV, respectively. Vinyl ($CHCH_2$) is the most abundant non-molecular C_2 species on $Fe_3C(100)$.

4. Conclusions

The detailed mechanism of C_2H_4 adsorption, dehydrogenation, and cleavage on $Fe_3C(100)$ was investigated using spin-polarized DFT and a periodic slab model. C_2H_4 adsorbs on surface Fe atoms by both C atoms, and the μ-bridging adsorption mode is more stable than the π and di-σ adsorption modes. The interaction of C_2H_4 with the $Fe_3C(100)$ surface leads to the partial rehybridization of the C atoms of C_2H_4 ($sp^2 \rightarrow sp^3$), resulting in the geometry of the C atom in C_2H_4 changing to be quasi-tetrahedron. The ethylene (C_2H_4) adsorption energy correlates with the degree of bending deformation of methylene (CH_2) on $Fe_3C(100)$. The four H atoms of ethylene (C_2H_4) are situated in different surface chemical environments, and each dehydrogenation step is different on $Fe_3C(100)$. At high coverages, all five C_2H_4 adsorption configurations coexist. Dehydrogenation of the π adsorption configuration **a1** to form vinyl $CHCH_2$ (**b1**) and vinylidene CCH_2 (**b2**) is the most facile pathway. The first dehydrogenation step ($C_2H_4 \rightarrow CHCH_2 + H$) has a lower barrier of 0.34 eV and is slightly exothermic by 0.08 eV. The second dehydrogenation step ($CHCH_2 \rightarrow CCH_2 + H$) only needs a barrier of 0.06 eV and is exothermic by 0.27 eV. The following dehydrogenation of vinylidene CCH_2 (**b2**) needs to overcome a higher barrier of 1.10 eV, and it is also unfavorable thermodynamically. At low coverages, ethylene mainly adsorbs in the μ-bridging mode. The first two dehydrogenation steps of

Graphical Abstract

Chin. J. Catal., 2014, 35: 28–37 doi: 10.1016/S1872-2067(12)60703-7

Density functional theory study of the adsorption and reaction of C_2H_4 on $Fe_3C(100)$

Bingyin Wang, Xiaohu Yu, Chunfan Huo*, Jianguo Wang, Yongwang Li
Institute of Coal Chemistry, Chinese Academy of Sciences;
University of Chinese Academy of Sciences;
Synfuels China Co. Ltd

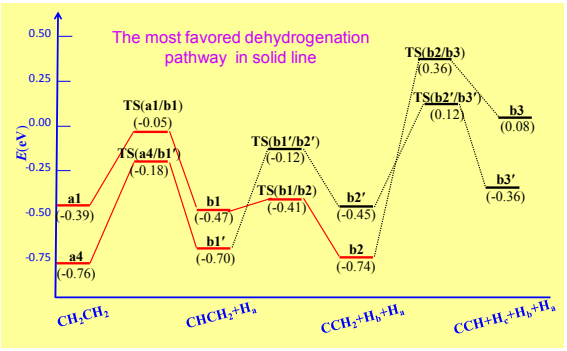

DFT calculations indicate that on $Fe_3C(100)$, C_2H_4 favors dehydrogenation reaction, while the C–C cleavage is not competitive. Vinylidene (CCH_2) and vinyl ($CHCH_2$) are the most abundant.

configuration **a4** have the same energy barrier of 0.58 eV and are slightly endothermic by 0.06 and 0.08 eV. The third dehydrogenation step is endothermic by 0.28 eV with a higher energy barrier of 0.74 eV. Therefore, vinyl ($CHCH_2$) and vinylidene (CCH_2) are the most abundant C_2 species on $Fe_3C(100)$, and it may be the major monomer of C_2H_4 that participates in the chain growth in FTS.

Acknowledgments

We greatly appreciate the equipment and fund support from Synfuels China Co., Ltd.

References

[1] Biloen P, Sachtler W M H. *Adv Catal*, 1981, 30: 165
[2] Wang Y, Kang J C, Zhang Q H. *Petrochem Technol* (王野, 康金灿, 张庆红. 石油化工), 2009, 38: 1255
[3] Davis B H. *Catal Today*, 2009, 141: 25
[4] Li S, O'Brien R J, Meitzner G D, Hamdeh H, Davis B H, Iglesia E. *Appl Catal A*, 2001, 219: 215
[5] de Smit E, Beale A M, Nikitenko S, Weckhuysen B M. *J Catal*, 2009, 262: 244
[6] Emmett P H. Crystallite Phase and Their Relationship to Fischer-Tropsch Catalysis. New York: Reinhold, 1956. 407
[7] Herranz T, Rojas S, Pérez-Alonso F J, Ojeda M, Terreros P, Fierro J L G. *J Catal*, 2006, 243: 199
[8] Mirzaei A A, Habipour R, Faizi M, Kashi E. *Appl Catal A*, 2006, 301: 272
[9] de Smit E, Cinquini F, Beale A M, Safonova O V, van Beek W, Sautet P, Weckhuysen B M. *J Am Chem Soc*, 2010, 132: 14928
[10] Schulz H. *Appl Catal A*, 1999, 186: 3
[11] Fischer F, Tropsch H. *Ber Deutsch Chem Ges*, 1926, 59: 830
[12] Scorch H H, Goulombic N, Anderson R B. The Fischer-Tropsch and Related Syntheses. New York: Wiley, 1951
[13] Kummer J T, Emmett P H. *J Am Chem Soc*, 1953, 75: 5177
[14] Pichler H, Schulz H. *Chem Ing Tech*, 1970, 42: 1162
[15] Ciobica I M, Frechard F, van Santen R A, Kleyn A W, Hafner J. *Chem Phys Lett*, 1999, 311: 185
[16] Huo C F, Li Y W, Wang J G, Jiao H J. *J Am Chem Soc*, 2009, 131: 14713
[17] Ciobica I M, Kramer G J, Ge Q, Neurock M, van Santen R A. *J Catal*, 2002, 212: 136
[18] Wu M C, Goodman D W. *J Am Chem Soc*, 1994, 116: 1364
[19] Wu M C, Goodman D W. *Surf Sci*, 1994, 306: L529
[20] Liu Z P, Hu P. *J Am Chem Soc*, 2002, 124: 11568
[21] Chen J, Liu Z P. *J Am Chem Soc*, 2008, 130: 7929
[22] Deng L J, Huo C F, Liu X W, Zhao X H, Li Y W, Wang J G, Jiao H J. *J Phys Chem C*, 2010, 114: 21585
[23] Krishna K R, Bell A T. *Catal Lett*, 1992, 14: 305
[24] Cao D B, Li Y W, Wang J G, Jiao H J. *J Mol Catal A*, 2011, 346: 55
[25] Turner M L, Byers P K, Long H C, Maitlis P M. *J Am Chem Soc*, 1993, 115: 4417
[26] Turner M L, Long H C, Shenton A, Byers P K, Maitlis P M. *Chem Eur J*, 1995, 1: 549
[27] Jordan D S, Bell A T. *J Phys Chem*, 1986, 90: 4797
[28] Mims C A, McCandlish L E, Melchior M T. *Catal Lett*, 1988, 1: 121
[29] Kresse G, Hafner J. *Phys Rev B*, 1993, 48: 13115
[30] Kresse G, Furthmüller J. *Comput Mater Sci*, 1996, 6: 15
[31] Kresse G, Furthmüller J. *Phys Rev B*, 1996, 54: 11169
[32] Perdew J P, Burke K, Ernzerhof M. *Phys Rev Lett*, 1996, 77: 3865
[33] Blöchl P E. *Phys Rev B*, 1994, 50: 17953
[34] Jónsson H, Mills G, Jacobsen K W. Classical and Quantum Dynamics in Condensed Phase Simulations. Singapore: World Scientific, 1998. 385
[35] Loffreda D, Delbecq F, Simon D, Sautet P. *J Phys Chem B*, 2001, 105: 3027
[36] Pallassana V, Neurock M, Lusvardi V S, Lerou J J, Kragten D D, van Santen R A. *J Phys Chem B*, 2002, 106: 1656
[37] Xing B, Wei Z Z, Wang G C. *J Energy Chem*, 2013, 22: 671
[38] van Santen R A, Neurock M, Shetty S G. *Chem Rev*, 2010, 110: 2005
[39] Jacobsen C J H, Dahl S, Clausen B S, Bahn S, Logadottir A, Nørskov J K. *J Am Chem Soc*, 2001, 123: 8404

C_2H_4在$Fe_3C(100)$表面吸附及脱氢裂解的密度泛函理论研究

王丙寅[a,b], 于小虎[a], 霍春芳[a,c,*], 王建国[a], 李永旺[a,c]
[a]中国科学院山西煤炭化学研究所煤转化国家重点实验室, 山西太原030001

[b]中国科学院大学, 北京100049
[c]中科合成油技术有限公司国家能源煤制液体燃料研发中心, 北京101407

摘要: 采用自旋极化密度泛函理论和周期平板模型, 对C_2H_4在铁基费托合成催化剂活性相之一Fe_3C(100)表面从热力学和动力学两个方面分析了C_2H_4在Fe_3C(100)表面进行脱氢和裂解反应的竞争性. 结果表明, C_2H_4在Fe_3C(100)表面的μ-bridging吸附比π、di-σ吸附更加稳定; C_2H_4与Fe_3C(100)面的相互作用导致C_2H_4的C原子部分发生重新杂化($sp^2 \rightarrow sp^3$), 使C原子呈近四面体结构. 在Fe_3C(100)表面C_2H_4易于发生脱氢反应, C–C键裂解反应不具有竞争性. 亚乙烯基CCH_2和乙烯基$CHCH_2$是Fe_3C(100)表面最丰的C_2物种, 或是C_2H_4参与链增长的主要单体形式.

关键词: 乙烯; 碳化铁; 吸附; 脱氢; 裂解; 费托合成; 密度泛函理论

收稿日期: 2013-07-29. 接受日期: 2013-09-02. 出版日期: 2014-01-20.
*通讯联系人. 电话: (010)69667589; 传真: (010)69667800; 电子信箱: hcf905@sxicc.ac.cn
基金来源: 国家重点基础研究发展计划(973计划, 2011CB201401); 国家自然科学基金(21273261).
本文的英文电子版由Elsevier出版社在ScienceDirect上出版(http://www.sciencedirect.com/science/journal/18722067).

1. 前言

费托合成(FTS)[1]是合成气($CO + H_2$)经催化反应转化为碳氢化合物的过程, 是煤、天然气和生物质等含碳资源间接转化为高品位液体燃料和化工原料的一个关键步骤. Fe基催化剂具有操作温度范围宽、时空收率和烯烃产量较高、WGS反应活性高及价格低廉等特点[2], 因而得到了广泛的研究和应用[3].

大量透射电子显微镜、X射线衍射和穆斯堡尔谱研究表明, 铁碳化合物是铁基费托催化剂主要活性相, 包括Fe_5C_2和Fe_3C等[4–9]. 近年来费托合成的实验和理论研究取得了很大的进展, 但是仍有不少关键科学问题亟待解决, 如碳链是如何增长的[10], 烯烃再吸附又是怎样影响产物分布的. 文献报道的链增长机理主要有三大类, 分别是碳化物机理[11]、烯醇机理[12,13]和CO插入机理[14]. C_xH_y物种在许多金属表面的存在[15,16]为由Fischer和Tropsch提出的碳化物机理提供了强有力的实验和理论依据.

在传统的碳化物机理中, CH_2被认为是最可能的链增长单体. 但近年来提出了许多不同的观点. Ciobica等[17]发现在Ru(0001)面, CH是最稳定的C_1物种,据此提出CH是链增长的可能单体, 与Wu等[18,19]的实验结果吻合. Liu等[20,21]使用密度泛函理论(DFT)研究了平坦和台阶的Ru(0001)及台阶的Rh(111)面上C–C偶合反应, 发现CH可能是链增长单体. Deng等[22]提出Fe_3C(100)表面最稳定的CH_x物种是CH. 大部分CH是由表面C原子加氢而来, 少量由CO氢助解离提供.

Krishna等[23]使用$^{13}CO/H_2$和$^{12}C_2H_4$研究了C_2H_4对链增长产物分布的影响, 发现C_2H_4再吸附可增加C_{3+}烃类化合物在产物中的比例. Cao等[24]利用DFT计算并提出, 在Fe_5C_2(001)表面来源于CCH_2和CHCH脱氢的CCH与C原子偶合形成CCCH. Turner等[25,26]和Jordan等[27]的实验表明, 乙烯基$CHCH_2$可能作为单体参与了碳氢化合物形成. Mims等[28]研究了Ru催化剂上高分子量碳氢化合物的形成, 提出亚乙烯基(CCH_2)可能是C_2物种的稳定单体.

本文采用DFT和周期平板模型, 从热力学和动力学角度研究了C_2H_4在Fe_3C(100)表面的吸附、脱氢和裂解反应, 力求阐释烯烃再吸附及其参与链增长的可能形式, 为基于详细机理的动力学研究提供理论指导.

2. 计算方法和模型

本文计算使用基于平面波DFT的VASP (Vienna Ab initio Simulation Package)[29–31]软件. 交换相关能用广义梯度近似(GGA)方法中的PBE (Perdew, Burke and Ernzerhof)[32]泛函来计算. 电子和离子相互作用通过缀加投影波PAW (projector augmented wave)函数来描述[33]. Kohn-Sham单电子采用平面波基组展开, 截断能设为400 eV. 由于自旋极化对于磁性材料的计算影响很大, 因此具有超顺磁性的Fe_3C采用自旋极化的方法来计算.

本文分别使用p(1×2)和p(2×2)的周期平板模型来研究C_2H_4在Fe_3C(100)表面的吸附和脱氢、裂解行为. 布里渊区采用1×3×1的K点描述. 为了消除层与层之间的相互作用, 真空层高度设为1.5 nm. 该模型是由8层Fe原子和4层C原子(8Fe+4C)组成的, 如图1所示.

在所有计算中均固定下面的6层Fe原子和3层C原子(6Fe+3C), 弛豫上面的2层Fe原子和1层C原子(2Fe+1C). 在计算能垒时, 采用CI-NEB方法搜寻过渡态[34]. 所有稳定的结构和过渡态均经频率分析进一步确认. 吸附能定义为: $E_{ads} = E(\text{adsorbates/slab}) - [E(\text{adsorbates}) + E(\text{slab})]$, 其中, $E(\text{adsorbates/slab})$是物种吸附在表面上的总能量, $E(\text{adsorbates})$是自由物种的总能量, $E(\text{slab})$是洁净表面

的总能量. 反应前后的反应热及反应能垒分别用$\Delta_r E$和E_a来表示: $\Delta_r E = E(\mathrm{FS}) - E(\mathrm{IS})$, $E_a = E(\mathrm{TS}) - E(\mathrm{IS})$. 其中$E$(IS), E(TS)和E(FS)分别代表反应物(IS)、过渡态(TS)和产物(FS)的总能量.

3. 结果与讨论

3.1. C_2H_4的吸附

本文系统考察了C_2H_4在Fe_3C(100)表面所有可能位点的吸附, 其吸附构型有π, di-σ和μ-bridging三种模式, 计算所得的稳定吸附构型、重要键参数和吸附能见图2.

构型**a1**, **a2**和**a3**中C_2H_4以π方式吸附在暴露的第一层Fe原子上. C_2H_4的C和H原子仍近似在同一个平面内, 此时两个C原子与底物的同一个Fe原子成键, 形成C-Fe-C三元环结构的σ-π复合物[35]. 三种构型的吸附能分别为–0.39, –0.52和–0.53 eV. 相对于气相C_2H_4分子的C–C键长(0.1330nm), 吸附后的C_2H_4的C–C键(0.1426, 0.1414和0.1412 nm)均有所拉长, 表明C–C键强度有所弱化. 由于Fe_3C(100)表面并不平坦, 构型**a2**中吸附的C_2H_4分子略倾斜, 使得其中一个C原子和与表面C相连的Fe原子发生作用, 得到类di-σ吸附构型**a5**. 在该构型中, C–C键(0.1439 nm)被进一步弱化. 该构型的吸附能为–0.58 eV, 与**a2**和**a3**非常接近, 分别仅相差–0.06和–0.05 eV. 在构型**a4**中, C_2H_4的两个C原子均以桥式吸附在第一层和第二层Fe原子上, 形成 μ-bridging吸附. 其吸附能为–0.76 eV, 是C_2H_4在Fe_3C(100)表面最稳定的吸附构型. 其C–C键长为0.1480 nm, 伸长活化程度最大, 介于C_2H_4 (0.1330 nm)和C_2H_6 (0.1540 nm)之间. 四个H原子明显背离C–C平面, ∠HCC为114°, 介于C_2H_4 (121°)和C_2H_6 (111°)之间. 由此可见, 以μ-bridging位吸附的C_2H_4分子中C原子的杂化方式由sp^2部分转化为sp^3, 使C原子呈近四面体结构.

综上所述, 乙烯分子在Fe_3C(100)表面的吸附作用比较弱, 且μ-bridging吸附比π和di-σ方式稳定, C–C双键拉长活化程度最大, 与C_2H_4在纯金属表面的吸附性质相似[36,37]. 在低覆盖度下, C_2H_4主要以μ-bridging吸附形式**a4**存在. 在高覆盖度下, C_2H_4的5种吸附形式都可能存在. 乙烯分子的最高占据轨道(HOMO)是成键π轨道, 而最低空轨道(LUMO)是反键π*轨道. 乙烯吸附在Fe原子上时, 将成键π轨道上的部分电子转移给Fe原子的3*d*空轨道. 同时, 其反键π*轨道能量降低, 接受Fe原子3*d*轨道的反馈电子. 两种作用都会增强表面与乙烯的作用强度, 削弱乙烯的C=C双键, 导致键长伸长, 键级降低.

3.2. C_2H_4在Fe_3C(100)表面的脱氢及裂解

C_2H_4在Fe_3C(100)表面的脱氢和C–C裂解是竞争反应. 文献报道, 许多表面反应符合BEP关系[38,39], 即吸附较弱的构型具有较强的反应活性. 另一方面, 吸附强的构型具有高的浓度. 因此, 我们选取了π吸附方式的**a1**构型(图2**a1**)及μ-bridging吸附方式的**a4**构型(图2**a4**), 考察了C_2H_4在Fe_3C(100)表面的逐步脱氢和裂解过程. 由于构型**a2**, **a3**与**a1**的吸附方式相同, **a5**可由**a2**变形而得, 因此, **a2**, **a3**和**a5**应具有与**a1**相似的反应行为. 表1列出了各种可能基元反应的反应能垒和反应能, 每一步最优脱氢方式和裂解反应所涉及到的中间物种及过渡态结构见图3.

3.2.1. 构型**a1**的C_2H_4脱氢及裂解

由于C_2H_4中的4个H原子所处的表面环境不同, 使得每一步脱氢都具有选择性. 由表1可见, 以构型**a1**为起始点, 脱去$H_{a\text{-}d}$中一个H原子($C_2H_4 \rightarrow C_2H_3 + H$)的难易程度存在很大差异. 其中, 脱去$H_a$是动力学最有利的过程, 其能垒为0.34 eV, 反应轻微放热0.08 eV. 在对应过渡态**TS(a1/b1)**中, C_1–H_a键长由初始吸附态的0.1095 nm拉长到0.1541 nm, H_a原子以顶位方式吸附到Fe原子上, Fe–H_a键长为0.1611 nm. 终态**b1**中, H原子以三配位形式吸附在第一层和第二层Fe原子上, 其Fe–H_a键长为0.1744, 0.1784和0.1880 nm. **a1**裂解过程($C_2H_4 \rightarrow 2CH_2$)的反应能垒为1.55 eV. 在过渡态**TS(a1/c1)**中, C–C键由初始吸附态的0.1414 nm伸长到0.2393 nm, 在终态**c1**中C–C键彻底断裂, CH_2吸附在由一个第一层Fe原子和两个第二层Fe原子构成的三配位洞位上, C–C键断裂伴随着放出0.18 eV的热量. 由以上分析可知, C_2H_4(**a1**)在Fe_3C(100)表面首先会发生脱氢反应生成吸附态的$CHCH_2$物种(**b1**).

与C_2H_4第一步脱氢和裂解反应相比, **b1**对应的脱氢($C_2H_3 \rightarrow C_2H_2 + H$)和裂解过程($C_2H_3 \rightarrow CH_2 + CH$)能垒显著降低(0.06相比于0.47 eV, 0.55相比于1.50 eV, 0.67相比于1.55 eV), 且H_b原子的脱除在动力学上最有利. $CHCH_2$ (**b1**)中CH端向表面倾斜促进了C–H键的活化, 在相应过渡态**TS(b1/b2)**中, C_1–H_b键长由中间吸附态**b1**的0.1195 nm伸长到0.1559 nm, H_b原子以顶位吸附在表面Fe原子上, Fe–H键长为0.1602 nm. 终态**b2**时, H_b原子以三配位形式吸附在第一层和第二层Fe原子上, Fe–H键长为0.1691, 0.1710和0.1897 nm. 该步反应能垒仅为0.06 eV, 放热0.27 eV, 形成$\eta^3\eta^1$(C,C)吸附的CCH_2物种. 在**b1**裂解反应($C_2H_3 \rightarrow CH_2 + CH$)的过渡态**TS(b1/c2)**中,

C–C键长由0.1400 nm伸长到0.2474 nm, 反应能垒为0.67 eV. 在终态**c2**中C–C键彻底断裂, 形成三配位吸附的CH和CH_2物种, C–C键断裂伴随着放出0.35 eV的热量.

相对于过C–C键的垂直面构型**b2** (CCH_2)近似对称, 因此脱除H_c和H_d ($CCH_2 \rightarrow CCH + H$)的能垒(1.10和1.12 eV)和反应能(0.80和0.80 eV)非常相近. 在对应过渡态**TS(b2/b3)**中, C_2–H_c键由0.1087 nm伸长到0.1696 nm, H_c原子以顶位方式吸附到Fe原子上, Fe–H键长为0.1533 nm. 在终态**b3**中, CCH物种以$\eta^3\eta^1$(C,C)吸附, H_c原子以三配位形式吸附, Fe–H键长分别为0.1700, 0.1823和0.1971 nm. **b2**的裂解反应($CCH_2 \rightarrow C + CH_2$)能垒是1.69 eV. 在过渡态**TS(b2/c3)**中, C–C键由初始吸附态的0.1401 nm伸长到0.2325 nm. 在终态的裂解产物**c3**中, C和CH_2吸附在分别由一个第一层Fe原子与两个第二层Fe原子和由两个第一层Fe原子与一个第二层Fe原子构成的η^3位上, 反应吸热0.81 eV.

从构型**a1**脱氢和裂解的势能面曲线(图4)可以看出, C_2H_4在Fe_3C(100)表面易于发生脱氢反应, C–C键裂解反应不具有竞争性, CCH_2是最稳定的表面C_2物种. C_2H_4脱第一个(0.34 eV)和第二个H原子的能垒(0.06 eV)都较低, 但CCH_2继续脱氢是比较困难的, 需要克服较高的能垒(1.10 eV), 且吸热0.80 eV. 这表明在通常费托反应条件下, CCH_2难以进行脱氢反应; 相反, CCH物种很容易加氢(能垒仅为0.30 eV, 放热0.80 eV)生成CCH_2物种.

3.2.2. 构型a4的C_2H_4脱氢及裂解

以构型**a4**为起点, 第一步脱去H_a ($C_2H_4 \rightarrow C_2H_3 + H_a$)是动力学最有利的过程, 其能垒为0.58 eV (表1). 开始脱氢时H_a渐渐远离C_1原子, 倾斜到表面与Fe原子成键. 在过渡态**TS(a4/b1′)**中, H原子以顶位方式吸附在表面Fe原子上, Fe–H_a键长为0.1598 nm, C_1–H_a键长由初始吸附态的0.1134 nm伸长至0.1542 nm. 在终态**b1′**中H_a原子以三配位形式吸附在第一层和第二层Fe原子上, Fe–H_a键长分别为0.1741、0.1841和0.1851 nm. 整个反应是一个吸热0.06 eV的过程. **a4**的裂解反应($C_2H_4 \rightarrow 2CH_2$)能垒为1.40 eV, 过渡态**TS(a4/c1′)**时C–C键由初始吸附态的0.1480 nm伸长到0.2381 nm, 在终态**c1′**中C–C键彻底断裂, 形成1个三配位和1个桥式吸附的CH_2物种, C–C键断裂伴随着吸收1.13 eV的热量. 因此, C_2H_4 (**a4**)在Fe_3C(100)表面首先发生脱氢反应生成吸附态的$CHCH_2$物种(**b1′**).

$CHCH_2$ (**b1′**)继续脱去H_b生成CCH_2 (**b2′**)比脱去H_c生成CHCH (**b2″**)的能垒略低(0.58相比于0.62 eV). 在**b1′**脱H_b原子的过渡态**TS(b1′/b2′)**中, C_1–H_b键长由初始吸附态的0.1110 nm伸长到0.1738 nm, H_b与表面相邻的Fe原子成顶位吸附, 其Fe–H_b键键长为0.1546 nm. 在终态**b2′**中, H_b原子以三配位形式吸附在第一层Fe原子上, Fe–H_b键长分别为0.1704, 0.1877和0.1987 nm. 产物CCH_2的生成需要吸收0.08 eV的热量. 在**b1′**裂解($C_2H_3 \rightarrow CH_2 + CH$)过程的过渡态**TS(b1′/c2′)**中, C–C键长由初始吸附态的0.1477 nm伸长到0.1956 nm, 在终态**c2′**中C–C键彻底断裂. CH_2与1个第一层Fe原子和1个第二层Fe原子成桥式吸附, CH与两个第一层Fe原子和1个第二层Fe原子成三配位吸附. 其反应能垒为0.74 eV, 反应过程需吸收0.38 eV的能量.

构型**a4**脱H_b后的产物**b2′**以$\eta^2\eta^3$(C,C)形式吸附在Fe_3C(100)表面, 其H_c和H_d原子所处的表面环境不同, 因此脱除H_c和H_d ($CCH_2 \rightarrow CCH + H$)的难易程度不同, 其能垒分别为0.74和0.92 eV. 在对应过渡态**TS(b2′/b3′)**中, C_2–H_c键由0.1107 nm伸长到0.1706 nm, H_c原子移动到Fe原子顶位上, Fe–H_c键长为0.1648 nm. 在终态**b3′**中, CCH物种以$\eta^3\eta^3$(C,C)吸附, H_c原子吸附在两个第一层Fe原子和一个第二层Fe原子构成的三配位上, Fe–H_c键长分别为0.1721, 0.1873和0.1926 nm. 生成产物CCH需要吸收0.28 eV的热量. **b2′**的裂解反应($CCH_2 \rightarrow C + CH_2$)能垒为0.88 eV. 在过渡态**TS(b2′/c3′)**中, C–C键由初始吸附态的0.1438 nm伸长到0.2044 nm. 在终态的裂解产物**c3′**中, C和CH_2分别吸附在由两个第一层Fe原子与两个第二层Fe原子构成的四配位上和由第一层Fe原子与第二层Fe原子构成的桥位上, 反应吸热0.81 eV.

从μ-bridging吸附构型**a4**在Fe_3C(100)表面进行脱氢和裂解反应的势能面曲线(图5)可以看出, C_2H_4的C–C裂解反应能垒远远高于脱氢反应, 因而后者更容易发生. 前三步脱氢反应能垒较接近(0.58, 0.58和0.74 eV), 且分别吸热0.06, 0.08和0.28 eV. $CHCH_2$是表面最丰的非分子态C2物种.

4. 结论

采用DFT方法和周期平板模型, 对C_2H_4在Fe_3C(100)表面的吸附及脱氢裂解进行了详细的考察. 研究表明, C_2H_4两个C原子吸附在Fe_3C(100)表面的Fe原子上, 且μ-bridging吸附比π, di-σ吸附更加稳定. C_2H_4与Fe_3C(100)面作用导致C_2H_4的C原子部分发生重新杂化($sp^2 \rightarrow sp^3$), 使C原子呈近四面体结构. C_2H_4在Fe_3C(100)表面的吸附能与其亚甲基CH_2在表面弯曲变形程度有关

系. 由于C_2H_4分子中4个H原子所处的表面化学环境不同, 使得每一步脱氢具有一定的选择性. 在高覆盖度下, C_2H_4的5种吸附形式都可能存在. π吸附构型**a1**更容易发生脱氢反应生成$CHCH_2$(**b1**)和CCH_2(**b2**). 第一步脱氢($C_2H_4 \rightarrow CHCH_2 + H$)能垒为0.34 eV, 反应轻微放热0.08 eV. 第二步脱氢($CHCH_2 \rightarrow CCH_2 + H$)能垒仅为0.06 eV, 反应放热0.27 eV. CCH_2(**b2**)继续脱氢具有较高的能垒(1.10 eV), 且热力学上也是不利的. 在低覆盖度下, C_2H_4主要以μ-bridging吸附形式**a4**存在. 构型**a4**的前两步脱氢能垒为0.58 eV, 轻微吸热0.06和0.08 eV, 第三步脱氢能垒略高(0.74 eV), 吸热0.28 eV. 综合以上分析, CCH_2和$CHCH_2$是Fe_3C(100)表面最丰的C_2物种, 或是C_2H_4参与链增长的主要单体形式.

致谢 感谢中科合成油技术有限公司在设备和资金上的支持.